Available online at www.sciencedirect.com

ScienceDirect

Procedia Materials Science 3 (2014) 1736 – 1741

Procedia Materials Science

www.elsevier.com/locate/procedia

20th European Conference on Fracture (ECF20)

Changes of work function in different deformation stage for 2205 duplex stainless steel by SKPFM

R. J. Wang[a], J. X. Li[a]*, Y. J. Su[a], L. J. Qiao[a], Alex A. Volinsky[b]

[a]*Corrosion and Protection Center, Key Laboratory for Environmental Fracture (MOE), University of Science and Technology Beijing, Beijing 100083*

[b]*Department of Mechanical Engineering, University of South Florida, Tampa, FL 33620, USA*

Abstract

The surface topography and potential changes of the 2205 duplex stainless steel due to tensile deformation were investigated by the in situ scanning Kelvin probe force microscopy. The slip bands generated by tensile deformation could decrease the surface potential. The surface roughness and the work function increased with deformation in the elastic region and reached the maximum values at the yield point. In the plastic deformation stage, the surface roughness continued to increase, while the work function decreased and stabilized. The surface roughness is the major factor affecting the work function during elastic deformation, while dislocations and slip bands play the key role during plastic deformation.

Selection and peer-review under responsibility of the Norwegian University of Science and Technology (NTNU), Department of Structural Engineering

Keywords: SKPFM; work function; elastic deformation; plastic deformation; surface roughness

1. Introduction

Kelvin probe is a method of measuring electron work function of the metal surfaces in air or in vacuum. In 1898 Lord Kelvin proposed the method after Stratmann [1,2] to study the atmospheric corrosion, and since 1980s, the technology has been widely used in the field of corrosion. Nonnenmacher et al. [3] combined scanning Kelvin probe (SKP) and atomic force microscopy (AFM), and called it Kelvin probe force microscopy (KFM), which can

* Corresponding author. Tel.: +86-10-62334493; fax: +86-10-62332345.
E-mail address: jxli65@ustb.edu.cn (J. X. Li)

Selection and peer-review under responsibility of the Norwegian University of Science and Technology (NTNU), Department of Structural Engineering
doi:10.1016/j.mspro.2014.06.280

simultaneously detect the surface morphology and potential distribution of the metal surface. In the recent 10 years, the technique of combining SKP and AFM has been used many times and the scanning Kelvin probe force microscopy (SKPFM) was put forward, as it can not only measure the surface morphology of the sample, but also detect the potential difference between the probe tip and the sample surface. In the field of corrosion and electrochemistry, SKPFM has been used to study various alloy pitting and corrosion behavior of the secondary phase [4-9]. During the SKPFM measurements, an AC voltage is applied to the tip to induce a harmonic oscillation of the cantilever in the presence of potential difference between the tip and the sample, measured by normal AFM detection scheme. After that, a reverse DC voltage with the same magnitude is applied to the tip to stop the oscillation and reduce the potential polarity. In SKPFM, the contact potential difference (CPD) between the tip and the sample was directly measured [10]. The work function (WF) is the minimum energy required for the electron to move from the Fermi level to the solid surface. Solid materials with free electrons have specific band structure and Fermi levels. The material microstructure will change when the temperature, stress and electric fields change, causing the internal electron migration or transition. Both experiments and theory indicate that the WF is closely related to the material corrosion potential. For example, Schmutz found that there is a linear relationship between the corrosion potential and the surface potential measured by SKPFM in Al alloys [11-14]. Leblanc [15] and Li [16] also found that the WF is very sensitive to corrosion behavior.

Study of Li et al. [16,17] also showed that the WF decreased with the strain and became stable when the strain reached a certain level. The WF of Cu decreased with the surface roughness in the sliding wear process. Levitin [18] calculated the WFs in Al, Ti, Fe and Ni single crystals undergoing tensile strain by using the density functional method. The experimental and theoretical results show that the WF decreased with the tensile strain. However, Loskuto [19] pointed out that the WF in Al increased with the strain due to the crystal surface relaxation, based on the self-consistent calculations. The research results of Xue [20] showed that the WF in Al alloy increased with the surface roughness.

The WF is one of the basic characteristics of the solid surface, as it reflects the electron energy level. Previous studies explained the WF changes with strain based on the increased number of dislocations, or changes of the surface roughness. In this paper, changes of the duplex stainless steel (DSS) WF were characterized at three deformation stages: small elastic deformation, large elastic deformation and plastic deformation stages. The effects of dislocations and the surface roughness on the WF were systematically studied, trying to find the main factor affecting the WF at different deformation stages.

2. Materials and experimental methods

The material tested is 2205 duplex stainless steel, with the following composition in wt.%: Cr 22.2%, Ni 5.48%, Mo 3.31%, Si 0.46%, Mn 1.28%, C 0.039%, P 0.016%, S 0.0013%, N 0.20%. Two types of specimens were utilized. The first type is the loading device (Patent No: ZL201320226066.3 Chinese patent), with the gauge size of 4 mm×3 mm×0.3 mm, named Sample 1. The second type is the tensile sample which the gauge size of 4 mm×3 mm×1 mm. The second type samples were subjected to small and large applied pre-strain, named Sample 2 and Sample 3, respectively.

The Sample 1 was loaded by screwing in the bolt, and the deformation magnitude was calculated from the bolt rotating angle. Sample 1 was deformed elastically (small elastic tensile deformation). Sample 2 and Sample 3 were loaded by the tensile testing machine NOML-1. The Sample 2 was loaded in the range of large elastic to plastic deformation, and the Sample 3 was loaded in plastic deformation regime. Sample 2 and Sample 3 were tested by SKPFM immediately after unloading.

SKPFM measurements of the DSS specimens were acquired using a dimension AFM (Nanoscope, Veeco Instruments Inc) operated in the tapping mode. Magnetic force microscopy (MFM) is capable of distinguishing paramagnetic austenite and ferromagnetic ferrite phases. Thus, the austenite and ferrite phases were differentiated using this method. To accurately observe the changes of the surface potential caused by tensile deformation, the sample surface should be very smooth. In order to eliminate the residual deformation caused by the mechanical polishing, the surface of each sample was wet ground with the SiC paper up to 5000 grit, polished using 0.5 μm diamond paste, and then ultrasonically cleaned in acetone and ethanol for 15 min.

3. Results

The screw-loaded Sample 1 was tested five times by consequently increasing the strain up to 4.5%. This was considered the elastic deformation stage. Each time the strained sample surface was characterized by AFM. Sample 2 was pre-strained five times and observed by AFM immediately after unloading each time. The initial strain was 5%, while the maximum strain was 10%. This was considered the large elastic deformation stage. Sample 3 was also pre-strained five times. Initial strain was 9%, while the maximum strain was 20%, called the plastic deformation stage. The strains for Sample 2 and Sample 3 were loading strain, i.e. the sample unloaded elastically.

3.1. WF at small elastic deformation stage

Surface topography and potential images along with the surface topography profiles of the Sample 1 before loading and with 4.5% strain are shown in Figure 1. In SKPFM image the light regions are austenite, while the dark regions are ferrite. With the 4.5% strain, Sample 1 was in elastically deformed, exhibiting embossed surface appeared in Fig.1(c), compared with Fig.1(a). SKPFM images in Fig.1(b) and (d) show almost no difference before and after deformation. Topography profile of the deformed sample in Fig.1(f) shows much rougher embossed surface, compared with the smoother un-deformed sample surface profile in Fig.1(e).

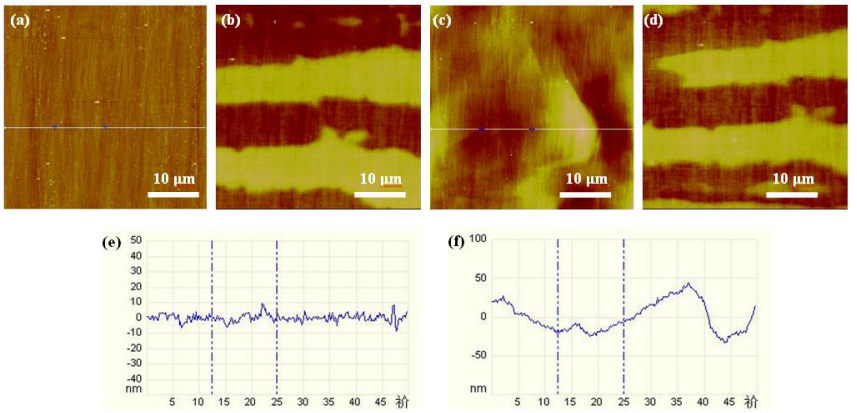

Fig. 1. (a) The surface topography and (b) the surface potential image of the Sample 1 before tensile loading; (c) The surface topography and (d) the surface potential image of the Sample 1 with 4.5% strain; (e) The surface topography profile along the scan line in (a); (f) The surface topography profile along the scan line in (c).

Higher contrast of the surface topography means that the surface roughness increased. Five ranges of the surface roughness under different strains are shown in Table 1. The surface roughness increased with strain.

In SKPFM, the CPD between the tip and the sample is defined as:

$$eV_{CPD}=\Psi_{tip}-\Psi_{sample} \tag{1}$$

where Ψ_{tip} and Ψ_{sample} are the WFs of the tip and the sample, and e is the electron charge. Given the WF of the tip, Ψ_{tip}, the WF of the sample, Ψ_{sample}, can be calculated. The obtained potential values are also related to the tip characteristics, such as the metal coating and the probe geometry [1, 21]. In order to avoid the corresponding errors, the potential measurements were initially calibrated using pure Ni, since its surface potential is very stable. V_{CPD} for pure Ni was calculated as -0.264 mV, and according to the equation (1), Ψ_{tip} was obtained as 4.886 eV. CPD measurements were performed on the strained samples from the α and γ phases. The measured CPD vales in Table 1 were converted to the WF using equation (1). Table 1 shows that both the surface roughness and the WF increased with the tensile strain in the small elastic deformation stage of the Sample 1.

Table 1. The surface roughness and WF of the 2205 DSS at different strain levels at small elastic deformation stage (Sample 1).

Screw disp., mm		0	0.12	0.13	0.14	0.17	0.18
Strain, %		0	3	3.3	3.5	4.3	4.5
Roughness, Ra, nm		1.7	6.8	9.6	9.7	10.5	12
WF, eV	α	5.264	5.275	5.266	5.279	5.294	5.296
	γ	5.290	5.299	5.290	5.301	5.312	5.319

3.2. WF at the large elastic deformation stage

Figure 2 shows the surface topography and potential images, along with the line profiles of the surface potential of the un-deformed and deformed Sample 2. In Fig. 2 the strain of about 10% is between the linear and the plastic regions of the stress-strain curve, thus the Sample 2 was deformed close to the yield point. Fig.2(a) shows the surface topography of the un-deformed Sample 2, while Fig.2(d) is the surface topography after 9% tensile strain with the slip bands in the austenite phase, pointed by the arrow. Corresponding SKPFM images in Fig.2(b) and (e) are different. In Fig.2(e), the region corresponding to the slip bands in Fig.2(d) can be clearly seen. Surface potentials before and after deformation are shown in Fig.2(c) and (e), corresponding to the white lines in SKPFM images in Fig.2(b) and (e). The surface potential decreased significantly after deformation in the slip bands region.

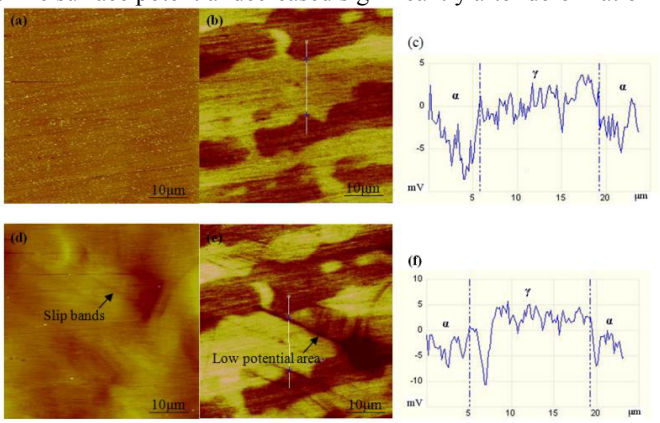

Fig. 2. Surface topography of undeformed (a) and deformed (d); surface potential image of undeformed (b) and deformed (e); the profile of the surface potential along the line on the SKPFM image for undeformed (c) and deformed (f) Sample 2 with 9% elongation.

Fig.2 shows that the silp bands observed in the surface topography correspond to the low potential region in the SKPFM image. It indicted that slip bands coresond to the low potential area. Slip band are formed by dislocations emergiung at the sample surface. Electrons are activated and escape easily because of the defects in the slip bands. The CPD between the tip and the sample was measurements for the α and γ phases, was turned into the WF, based on the equation (1). The surface roughness at different deformation levels increased with tensile deformation.

3.3. WF at the plastic deformation stage

Sample 3 was strained in the plastic deformation strain region, resulting in higher dislocation density and more slip bands in the topography image, which corresponding to the low potential area in the potential image. There is little change in the surface topography between the 12% and 20% strain.

Variations of the WF with strain for the three types of samples are shown in Figure 3. WF of the two phases increased with the strain for Samples 1 and 2. For the Sample 3, the WF of the two phases initially increased when the strain was less than 12%, then decreased and stabilized when the strain was greater than 12%.

The WF changes with the surface roughness and strain were consistent. The WF reached the maximum value in the middle of the tested strain range. According to the stress strain curve, this corresponds with the beginning of plastic deformation and yielding. Therefore, the surface roughness was the major factor affecting the WF in the elastic deformation stage. The surface roughness continued to slightly increase with the strain, while more dislocations and slip bands emerged at the surface, giving more chances for the electrons to escape from the sample surface. Thus, dislocations and slip bands played the key role in the plastic deformation stage.

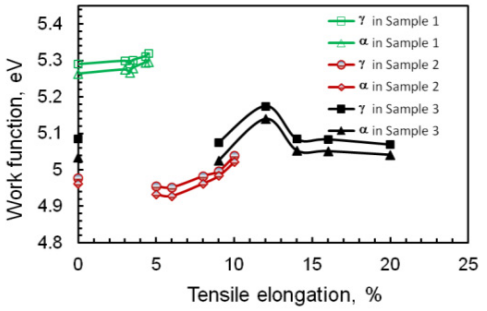

Fig. 3. Ferrite and austenite WF variation with the different deformation.

4. Discussion

Convex parts correspond to the peaks, while the concave parts correspond to the valley in the surface topography. Atoms are squeezed in the valleys and electrons are more tightly bound by the surrounding atoms, making it harder for the electrons to escape. Electrons can easier escape from the surface peaks due to reduced bonding. Zhou [23] studied the WF of materials in tension and compression. The result showed that the WF decreased with strain. The author also pointed out that the WF was affected by the surface roughness, while there was no surface roughness effect if the surface roughness did not reach a certain value. Unfortunately, the author did not offer the detailed data of the surface roughness in his study. Study of copper showed that the WF decreased and eventually reached a steady value with the surface roughness increase [24]. The surface roughness decreased slightly after annealing [25], and the result showed that the electrons were strongly bound after annealing, thus the WF slightly declined. In addition, studies have shown that the rougher the surface, the larger fluctuation in the WF would be, promoting the corrosion cell formation, which may explain why rougher surfaces are more prone to corrosion [24].

Li [16] found that the corrosion potential and the WF decreased with the increase of the corrosion rate in a study of the WF and corrosion behavior of deformed Cu, while corrosion rate increased with plastic strain. Strained surface was more electrochemically active. Corrosion potential and the WF tended to be stable, while the corrosion rate continued to increase when the plastic strain reached a certain level. The author believed that the increasing corrosion rate may be controlled by the dislocation density. Dislocations can lower the WF and the corrosion potential, while increasing the number of dislocations did not lead to decreased WF and corrosion potential. Various influencing factors on the WF achieved a relative balance with the increasing deformation.

This study shows that the surface roughness increased with strain in the elastic range, and changes of the WF were almost the same as with the surface roughness. In this work, the surface of each sample was wet ground with SiC paper up to 5000 grit, polished using diamond paste to 0.5 μm. There are basically no scratches on surface of sample, and the surface roughness is at the nano-scale, as shown in Fig.2. The smaller the nano-scale surface roughness, the weaker the electrons are bound by the surrounding atoms, so electrons have more chances to escape. With the increase of the surface roughness, topography peaks become smooth, and the surface electrons are more strongly bound, so that it is not easy for them to escape. The WF increased with the increasing nano-scale surface roughness, caused by tensile deformation. When sample enters the plastic deformation stage, surface roughness is more affected by the slip bands, caused by dislocations emerging at the surface. Surface electrons are weakly bound, thus they have more chances to escape away from the surface, which results in the lower WF. That is to say, dislocations or slip bands are the main factors affecting the WF in the plastic deformation stage. These results are identical to the results of Li [26].

It should be noticed that the WF of the Sample 1 is much higher than the Samples 2 and 3 because the Sample 1 was kept constant strain during the whole process of SKPFM observation and measurements. However, Samples 2 and 3 were pre-strained, i.e., they underwent elongation, but it was released.

In short, there are not only changes of the surface roughness, but also the formation of dislocations, which both affect the WF of deformed materials. It is important to consider which is the main factor affecting the WF of the surface at different deformation stages. The results show that the nano-scale surface roughness changes significantly, while there are not many dislocations formed during the small elastic deformation stage. Convex peaks change gradually from sharp to smooth, making it harder for electrons to escape, thus the WF increases gradually. In the plastic deformation stage, the number of dislocations increased rapidly and slip bands appeared on material surface, thus the surface potential obviously reduced in the slip bands, causing the WF to decrease.

5. Conclusions

In this work, variation of the surface roughness and the WF of 2205 duplex stainless steel were studied using SKPFM. The surface potential decreased significantly in the slip bands zone. The surface roughness and the WF increased with deformation in the elastic regime and reached the maximum value when deformed to the yield point. In the plastic deformation stage the surface roughness continued to increase, while the WF decreased and stabilized. The surface roughness is the major factor affecting the WF in the elastic regime, while dislocations and slip bands play the key role in the plastic regime.

Acknowledgements

This project was supported by the National Nature Science Foundation of China under Grant Nos. 51071025 and 51171024 and the 973 Program No. 2014CB643301.

References

[1] M. Stratmann. Corros. Sci, 1987; 27: 869–872
[2] M. Stratmann, H.Streckel. Corros. Sci, 1990; 30(6/7): 681–696
[3] M. Nonnenmacher, M. P. O'Boyle, H. K. Wickramasinghe. Applied Physics Letters, 1991; 58: 2921
[4] J.H.W. de Wit.Electrochimica Acta, 2001; 46: 3641
[5] J.H.W. de Wit. Electrochimica Acta, 2004; 49: 2841
[6] F. Andreatta, H. Terryn, J.H.W. de Wit. Electrochimica Acta, 2004; 49: 2851
[7] L.E. Fratila-Apachitei, I. Apachitei, J. Duszczyk. Electrochimica Acta, 2006; 51: 5892
[8] F. Andreatta, I. Apachitei, A.A. Kodentsov. Electrochimica Acta, 2006; 51: 3551
[9] A. Davoodi, J. Pan, C. Leygraf. Electrochimica Acta, 2007; 52(27): 7697
[10] S. Sadewasser, Th. Glatzel, M. Rusu, A. Jäger-Waldau, M.Ch. Lux-Steiner. Applied Physics Letters, 2002; 80: 2979–2981
[11] P. Schmutz, G.S. Frankel. J. Electrochem. Soc,1998; 145(7): 2285
[12] P. Schmutz, G.S. Frankel. J. Electrochem. Soc,1998; 145(7): 2295
[13] V. Guillaumin, P. Schmutz, G.S. Frankel. J. Electrochem. Soc, 2001; 148(5): B163–B173
[14] P. Schmutz, G.S. Frankel. J. Electrochem. Soc, 1999; 146(12): 4461
[15] P. Leblanc, G.S. Frankel. J. Electrochem. Soc, 2002; 149(6): B239
[16] W. Li, D.Y. Li. Applied Surface Science, 2005; 240: 388–395
[17] W. Li, D.Y. Li. Wear, 2003; 255: 333–340
[18] V.V. Levitin, O.L. Grin, V.K. Yatsenko. Vacuum, 2001; 63: 367.
[19] S.V. Loskuto, V.V. Pravda, Metalloved. Term. Obrab. Met, 1995; 9: 307.
[20] M.S. Xue, J. Xie, J.F. Ou. Journal of Nanchang Hangkong University, 2011; 25: 4
[21] M. Stratmann, F. Turcu. Corros. Sci, 2007; 53: 290–299
[22] M. Kochsiek. Metrologia , 1982; 18: 153–159
[23] Y. Zhou, J.Q. Lu, W.G. Qin. Materials Chemistry and Physics, 2009; 118: 12-14
[24] W. Li, D.Y. Li. Acta Materialia , 2006; 54: 445–452
[25] W. Li, D.Y. Li. J. Chem. Phys, 2005; 6: 122
[26] W. Li, D.Y. Li. Materials Science and Technology, 2002; 18: 1057–1060